
PLANesT-3D: A NEW ANNOTATED DATASET FOR SEGMENTATION OF 3D PLANT POINT CLOUDS

A PREPRINT

Kerem Mertoğlu
Faculty of Agriculture
Usak University
Usak, Turkey

Yusuf Şalk, Server Karahan Sarıkaya, Kaya Turgut
Department of Electrical-Electronics Engineering
Eskisehir Osmangazi University
Eskisehir, Turkey

Yasemin Evrenesoğlu
Faculty of Agriculture
Eskisehir Osmangazi University
Eskisehir, Turkey

Hakan Çevikalp
Department of Electrical-Electronics Engineering
Eskisehir Osmangazi University
Eskisehir, Turkey

Ömer Nezh Gerek
Department of Electrical-Electronics Engineering
Eskisehir Osmangazi University
Eskisehir, Turkey

Helin Dutagacı
Department of Electrical-Electronics Engineering
Eskisehir Osmangazi University
Eskisehir, Turkey
hdutagaci@ogu.edu.tr

David Rousseau
Laboratoire Angevin de Recherche en Ingénierie des Systèmes (LARIS)
Université d'Angers
Angers, France

August 1, 2024

ABSTRACT

Creation of new annotated public datasets is crucial in helping advances in 3D computer vision and machine learning meet their full potential for automatic interpretation of 3D plant models. In this paper, we introduce PLANesT-3D; a new annotated dataset of 3D color point clouds of plants. PLANesT-3D is composed of 34 point cloud models representing 34 real plants from three different plant species: *Capsicum annuum*, *Rosa kordana*, and *Ribes rubrum*. Both semantic labels in terms of "leaf" and "stem", and organ instance labels were manually annotated for the full point clouds. As an additional contribution, SP-LSCnet, a novel semantic segmentation method that is a combination of unsupervised superpoint extraction and a 3D point-based deep learning approach is introduced and evaluated on the new dataset. Two existing deep neural network architectures, PointNet++ and RoseSegNet were also tested on the point clouds of PLANesT-3D for semantic segmentation.

Keywords 3D point cloud · 3D plant modeling · 3D plant dataset · 3D semantic segmentation

1 Introduction

Cultivation of horticultural crops is one of the most labor-intensive economic activities, and is central to global food security [1, 2]. The accuracy and efficiency of horticultural practices, such as pruning, weed control, disease management, and harvesting directly influence the yield and quality of the crops [3]. The increasing global demand for high-quality crops, hence the demand for intensive labor motivates development of technologies for automation

in horticulture [4, 5]. Automated horticultural practices are expected to adapt to plant traits, which are diverse across plant species [6, 7]. Automation of trait measurements is also key to high throughput plant phenotyping, a fundamental process in plant research, breeding, and crop management [8–10]. Modeling of traits within a population, and capturing the structure of single plants or plant communities for particular operations have become major applications of computer vision [11–14].

3D computer vision is particularly relevant in many automated horticultural operations. Robotic systems designed to perform pruning, weeding, and harvesting require correct identification of plant parts, and accurate estimation of the location, size, shape, and orientation of the structures in 3D space [15–18]. Advances in 3D sensing technologies and machine learning fuel the development of algorithms for automatic segmentation of plants into their structural parts as well as organ-level trait estimation [19, 20].

Despite the considerable progress in 3D geometry modeling and analysis of plants in the last decades [21, 22], creation of benchmark datasets, a fundamental component for advancement of relevant research, is still lagging behind compared to other domains [23, 24]. Annotated public datasets of plant models are of particular importance both for comparison of competing algorithms and also for providing training data to machine learning processes [13].

Table 1: Public datasets containing full 3D models of plants in comparison with the PLANesT-3D dataset introduced in this work.

dataset	# models	Properties			
		Species	Modality	Color	Labels
Pheno4D [25]	126	Tomato Maize	Laser	No	Semantic & Instance
ROSE-X [26]	11	Rose	X-rays	No	Semantic
Plant3D [27] [28] [29]	714	Tomato Tobacco Sorghum Arabidopsis	Laser	No	Growth conditions
Soybean-MVS [30]	102	Soybean	MVS	Yes	Semantic & Instance
PLANesT-3D	34	Pepper Rose Ribes	SfM-MVS	Yes	Semantic & Instance

In the last decade, open datasets of annotated 2D plant images have been proliferated to assist evaluation of performance and development of machine learning models for plant phenotyping [31]. However, open datasets containing annotated and complete 3D plant models are rare. Table 1 gives a list of such existing datasets. Plant3D [27–29] contains a total of 714 3D laser scans of Tomato, Tobacco, Sorghum, and Arabidopsis plants obtained within 20–30 days of development. Information on the growth conditions of the plants are also provided. The 3D models do not contain color information. [32] manually labeled 54 models of the Plant3D data into stem and lamina points, and evaluated a range of machine learning approaches on this subset. [33] annotated 546 of the plants of the Plant3D dataset with semantic and instance labels. The labels are available upon request from [33]. ROSE-X dataset [26] contains 3D models of 11 rosebush plants acquired through X-ray computer tomography. The voxels in the volumetric models were labeled into three semantic categories: "Leaf", "Stem", and "Flower". The point cloud versions of the volumetric models are also available. Pheno4D [25] is a dataset of 3D point clouds of 7 maize plants and 7 tomato plants. The plants were scanned with a laser scanner at different growth stages resulting in 244 point clouds. 126 of them were manually annotated with semantic and instance labels. The Soybean-MVS dataset [30] is fundamentally different from the rest in terms of data acquisition modality. The plants were captured with an RGB camera in a controlled setup and their corresponding point clouds were created through multi-view stereo. A total of 102 point cloud models of five different soybean varieties were reconstructed at 13 stages of the whole growth period.

These 3D plant datasets have been often used for assessing off-the-shelf machine learning tools for semantic and instance segmentation [25, 30, 32, 34]. The datasets also enabled training and evaluation of new approaches specifically developed for plant data [35–38], including deep learning architectures such as PSegNet [33], PlantNet [39], RoseSegNet [40], and FF-Net [41].

Although smaller in terms of the number of models as compared to Pheno4D, Plant3D, and Soybean-MVS (Table 1), the new dataset (PLANesT-3D¹) introduced in this work contributes to the diversity of publicly available annotated 3D plant models in terms of acquisition modality, number of distinct plants, and inclusion of other species. The data is acquired with an RGB camera and reconstructed through structure from motion (SfM) and multi-view stereoscopy (MVS). Together with the Soybean-MVS dataset, the PLANesT-3D dataset will balance the dominant acquisition modality, which is laser scanning. Reconstruction with SfM and MVS does not require expensive equipment or elaborate acquisition setups, while yielding both geometric and textural information.

While Pheno4D and Soybean-MVS datasets are extremely valuable since they track the development of individual plants across time, the number of distinct plants are 14 for Pheno4D and 5 for Soybean-MVS. The PLANesT-3D dataset includes models of 34 distinct plants belonging to three species: namely *Capsicum annuum* (pepper), *Rosa kordana* (rose), and *Ribes rubrum* (ribes). Also, point clouds from two species (pepper and ribes), 3D models of which were not available before, are added to the public domain. The diversity of training and evaluation data in terms of acquisition modality, noise levels, plant species, plant instances, plant architecture, organ geometry, etc. plays an important role in assessing the robustness as well as the generalization ability of machine learning approaches.

The objective of this publication is twofold: First is to introduce PLANesT-3D, a new dataset containing complete 3D color point clouds of plants together with their semantic and instance labels. Second is to present a new segmentation approach, the SP-LSCnet, that combines an unsupervised clustering scheme and an adaptive network for point cloud classification. We also provide semantic segmentation results on the dataset with two point-based deep learning architectures, PointNet++ and RoseSegNet. The main contributions of this work can be summarized as follows:

1. We introduce PLANesT-3D, a new dataset containing RGB point clouds representing 34 real plants from three species.
2. We propose SP-LSCnet as a new semantic segmentation approach where an unsupervised clustering method based on t-distributed stochastic embedding (t-SNE) is combined with a point cloud classifier network. The classifier network employs two adaptive modules to adjust local region organization for feature extraction.
3. We tested RoseSegNet, a semantic segmentation algorithm we had previously developed for plant data [40] on the new dataset, and demonstrated that it is effective without requiring hyperparameter re-adjustment.

The rest of this article is organized as follows. In Sections 2.1 and 2.2, we describe the data acquisition, reconstruction, and pre-processing steps leading to the creation of 3D point clouds. We give detailed information about the PLANesT-3D dataset in Section 2.3. The segmentation methods evaluated in this work are described in Section 2.4. Our new segmentation approach, SP-LSCnet, is introduced in Section 2.4.1. The performances of the semantic segmentation methods on the PLANesT-3D dataset are reported in Section 3. A discussion of the work is provided in Section 4, followed by our conclusion in Section 5.

2 Materials and Methods

2.1 Data acquisition

In order to obtain full 3D plant models, 2D color images of 34 plants were acquired using a handheld DSLR camera (EOS 6D MARK II, Canon, Japan). The acquisition was performed on 10 potted pepper plants (*Capsicum annuum*), 10 potted rose plants (*Rosa kordana*), and 14 ribes plants (*Ribes rubrum*), planted directly to the soil in a greenhouse. Multiple color images of resolution 6240×4160 were captured manually around each plant via positioning the camera so as to cover as much plant surface as possible with a high degree of overlap. Three examples of the sets of camera locations and orientations are illustrated in Fig. 1.

Table 2 gives the number of images used to reconstruct the 3D plant point clouds. Three pairs of Ribes were very closely planted (Ribes 02 & 12, Ribes 04 & 13, Ribes 05 & 14). A single point cloud was reconstructed for each pair using the set of images where the pair appeared together. After reconstruction, noise removal and pose normalization, the two plants were manually segmented into separate point clouds of two individual plants.

2.2 Reconstruction and pre-processing of 3D point clouds

For reconstruction of 3D color point clouds from 2D color images, Agisoft Metashape Professional (Agisoft LLC, St. Petersburg, Russia) was employed. Agisoft Metashape is a software that performs photogrammetric processing of digital

¹The PLANesT-3D dataset is publicly available at <https://www.dropbox.com/s/8g10r0zo0j6kmdo/PLANesT-3D.rar?dl=0>

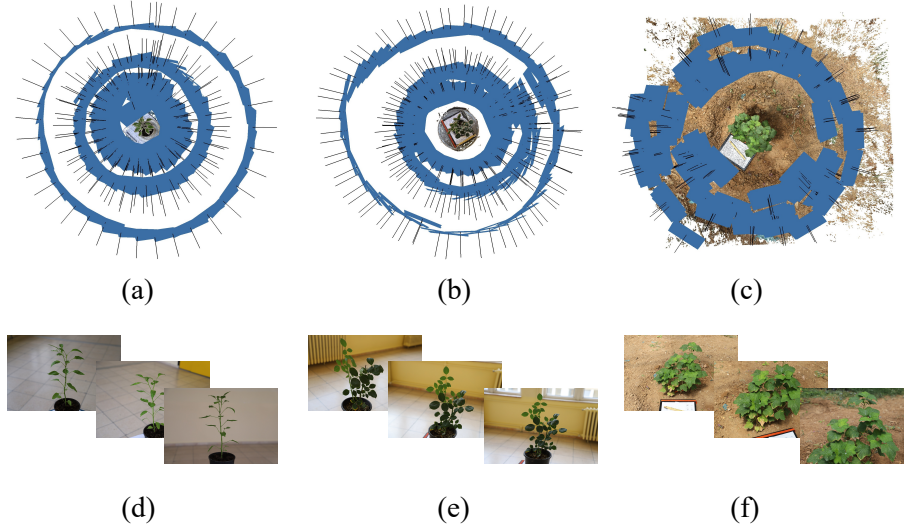


Figure 1: Estimated camera poses for 231 images of a pepper plant (a), 240 images of a rose plant (b), and 177 images of two ribes plants (c). Sample images for pepper (d), rose (e), and ribes (f) are also provided.

Table 2: Number of images used to reconstruct the 3D plant point clouds.

Plant ID	# images	Plant ID	# images	Plant ID	# images
Pepper 01	261	Rose 01	210	Ribes 01	243
Pepper 02	320	Rose 02	182	Ribes 02 & 12	177
Pepper 03	324	Rose 03	203	Ribes 03	294
Pepper 04	282	Rose 04	205	Ribes 04 & 13	235
Pepper 05	280	Rose 05	240	Ribes 05 & 14	169
Pepper 06	231	Rose 06	211	Ribes 06	150
Pepper 07	294	Rose 07	258	Ribes 07	225
Pepper 08	350	Rose 08	406	Ribes 08	222
Pepper 09	199	Rose 09	377	Ribes 09	191
Pepper 10	226	Rose 10	386	Ribes 10	310
				Ribes 11	240

images and generates 3D models through principles of structure from motion (SFM) and multi-view reconstruction [42]. Examples of the raw point clouds produced by Metashape Professional are given in Fig. 2. The software also provides confidence maps for the 3D points. The confidence value for a point corresponds to the number of images that "see" and contribute to reconstruct the point.

As can be observed from Fig. 2, the raw point clouds include structures from the background and are noisy. The correct scale of the scene is lost. Automatic segmentation of plants from each other and from the background is in itself a research problem. However, we aimed to provide a dataset of 3D models that correspond to isolated plants for evaluation of algorithms that focus on the analysis of single plants.

In order to recover the correct scale of the point cloud, remove background structures and noise, and segment the plant points from the scene, we devised a simple, semi-automatic procedure. We denote the raw point cloud as \mathcal{P}_R , where a point $p \in \mathcal{P}_R$ is represented by its coordinates $p = (x, y, z)$ defined in the coordinate frame returned by Metashape. The steps of the procedure are detailed as follows:

- **Recovering the scale:** The multiview reconstruction pipeline employed by Metashape Professional provides the scene geometry upto a scale, meaning that the correct scale of the structure is lost. To enable recovery of the correct scale, we installed rulers and objects with distinct patterns in the vicinity of the plants during image acquisition. Once the 3D point cloud is reconstructed, the markers on the rulers and on the patterns were picked manually. Let the set of these landmark points be $\{p_r\} \subset \mathcal{P}_R$ with $r = 1, 2, \dots, N_r$, where N_r is the number of landmark points. The distance between a pair of these reference points on the point cloud was

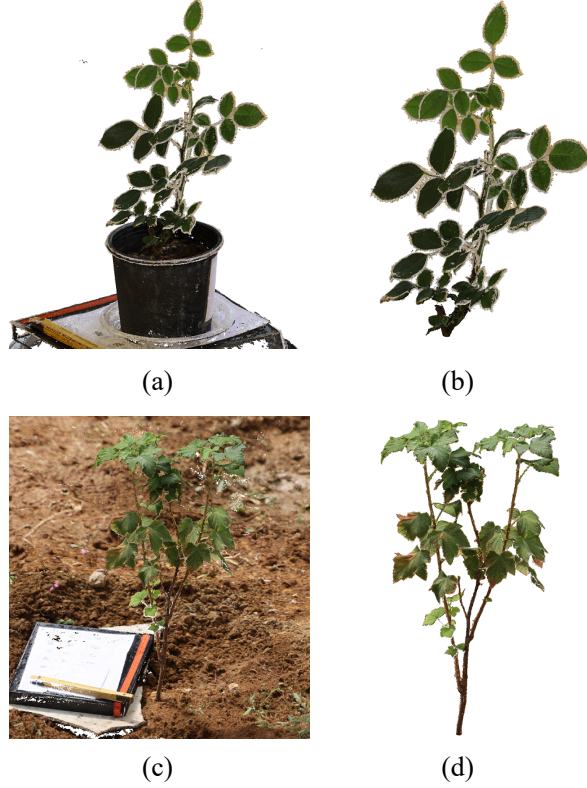


Figure 2: Raw point clouds reconstructed via Agisoft Metashape Professional of a rose plant (a) and a ribes plant (c). Corresponding clouds including only 3D points of the target plants are given in (b) for rose, and in (d) for ribes.

determined as $\hat{d}_{rs} = \|p_r - p_s\|$, where $\|\cdot\|$ corresponds to the Euclidean norm. The average of the distances of all the pairs is equal to

$$\hat{D}_R = \frac{1}{N_r(N_r - 1)} \sum_{r \neq s} \sum_s \hat{d}_{rs}. \quad (1)$$

Let D_R be calculated using the true metric distances (in cm units) between the landmark points d_{rs} measured manually, or read through the ruler. The scale factor is then determined as

$$S = \frac{D_R}{\hat{D}_R}. \quad (2)$$

The point cloud is scaled such that the average of the reference distances on the point cloud is equal to the measured distances on the real objects, i.e. the point coordinates were updated as $p' = S \cdot p$ for all $p \in \mathcal{P}_R$. The scaled point set is denoted as \mathcal{P}'_R .

- **Rotating the point cloud to a normalized pose:** We aimed to rotate the reference frame such that the XY-plane corresponded to the ground or the plane holding the plant pot. In order to estimate the parameters of this plane, we used M-estimator SAmple Consensus (MSAC) algorithm given in [43], which is a variant of RANdom SAmple Consensus (RANSAC) algorithm. We manually picked a point, p'_{base} , close to the plant base. Using the estimated normal vector $\mathbf{n} = [n_x, n_y, n_z]$ of the plane in the scene and the point p'_{base} at the plant base, we translated and rotated the point cloud \mathcal{P}'_R into a new reference frame using

$$\hat{p} = \mathbf{R}(p' - p'_{base}) \quad (3)$$

for all $p' \in \mathcal{P}'_R$. The point cloud rotated to this normalized pose is denoted as $\hat{\mathcal{P}}_R$. In Eq. 3, \mathbf{R} corresponds to the rotation matrix which transforms the normal \mathbf{n} to $[0, 0, 1]$ in the new reference frame. The origin of this reference frame corresponds to the hand-picked point at the plant base. The XY plane coincides with the plane detected by the MSAC algorithm. The positive Z-direction is oriented from the plant base towards the shoot.

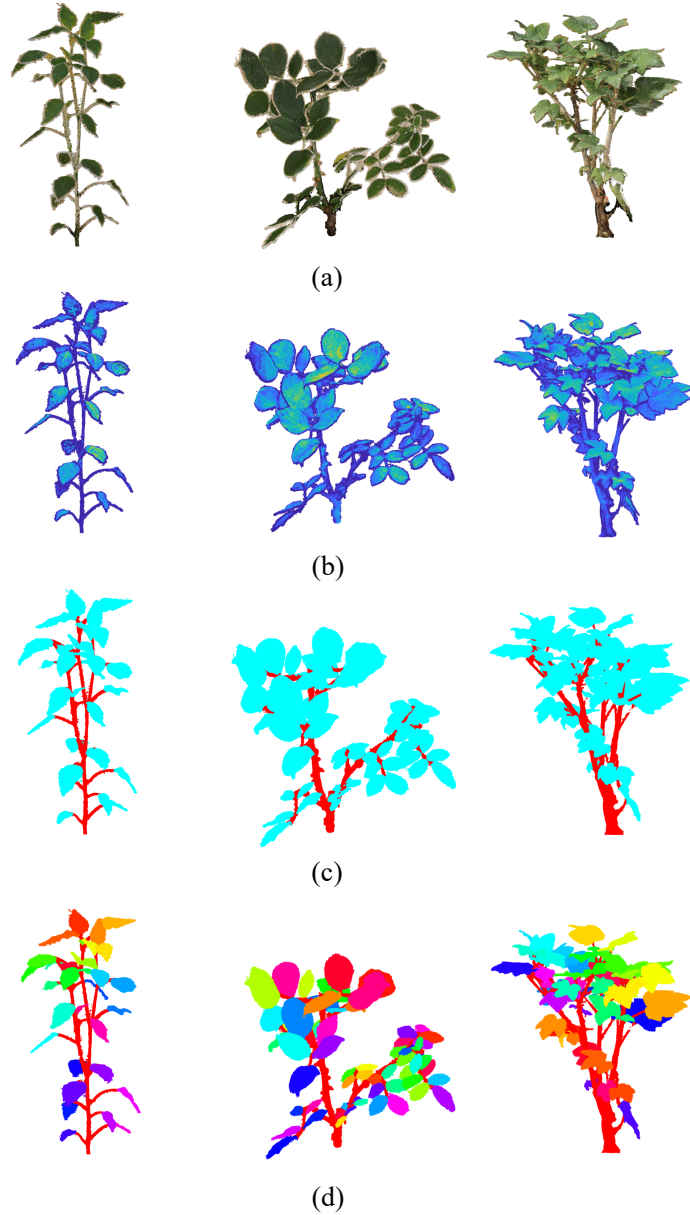


Figure 3: Three models from the PLANesT-3D dataset rendered with plant color (a), confidence map (b), semantic labels (c), and instance labels (d).

- **Extracting plant points:** Once the origin of the reference coordinate frame is established at the plant base, and the positive Z-direction points toward the plant shoot, we removed all points with a negative z coordinate, assuming all plant points remain above the plant base. We verified this assumption for all the models in the dataset. We applied connected component analysis to the rest of the point cloud and retained the points belonging to the largest connected component as the final plant point set $\mathcal{P} \subset \hat{\mathcal{P}}_R$. Examples of the outputs of this semi-automatic process is given in Fig. 2-(b) for a rose plant and in Fig. 2-(d) for a ribes plant.

2.3 The PLANesT-3D dataset

The PLANesT-3D dataset consists of 34 plant point clouds, where the plant points are isolated from the background as described in the previous section. Accompanying the locations and color information of the points in each model, three

scalar fields are provided: The confidence map as delivered by Metashape Professional, semantic labels, and instance labels. Examples of point clouds from the PLANesT-3D dataset and their corresponding confidence maps and labels are depicted in Fig. 3.

Both semantic labels and instance labels are obtained through manually labeling each point using CloudCompare point cloud processing software [44]. Semantic labels for PLANesT-3D correspond to "leaf" and "stem" classes. Points on the leaf blades were labeled as "leaf", main stem, branches, and petioles were included in the "stem" class. Instance labels are identity numbers representing individual leaflets within a plant model. All points labeled as "stem" were assigned a single instance label.

Table 3: Properties of the point clouds in PLANesT-3D

	Height (cm)	# points	"leaf" (%)	"stem" (%)	# leaflets
Pepper 01	53.63	2312959	70.45	29.56	33
Pepper 02	63.39	5531852	76.80	23.20	48
Pepper 03	60.65	3482959	72.43	27.57	45
Pepper 04	51.51	2425889	68.28	31.72	40
Pepper 05	48.95	2720311	69.52	30.48	35
Pepper 06	32.94	1846694	65.41	34.59	21
Pepper 07	49.71	1806010	69.11	30.89	27
Pepper 08	48.45	2311602	69.46	30.54	27
Pepper 09	53.32	3440529	74.10	25.90	38
Pepper 10	64.95	2416062	69.91	30.09	36
Rose 01	29.96	3452545	80.15	19.85	59
Rose 02	33.55	3601210	80.55	19.45	68
Rose 03	32.96	2580315	75.97	24.03	43
Rose 04	27.36	4091952	82.37	17.63	61
Rose 05	38.01	2867159	78.29	21.71	65
Rose 06	25.98	2540487	81.62	18.38	27
Rose 07	27.88	2999376	82.24	17.76	43
Rose 08	46.80	3616281	74.12	25.88	100
Rose 09	50.16	2119400	77.45	22.55	56
Rose 10	37.65	3296993	77.65	22.35	85
Ribes 01	76.92	2078729	88.33	11.67	64
Ribes 02	33.69	1299910	89.67	10.33	34
Ribes 03	74.25	1053341	84.32	15.68	33
Ribes 04	34.64	1190366	85.32	14.68	32
Ribes 05	104.85	1506387	78.09	21.91	105
Ribes 06	31.55	3175798	81.49	18.51	63
Ribes 07	93.66	3553784	85.66	14.34	101
Ribes 08	79.73	600792	67.04	32.96	41
Ribes 09	43.53	679885	68.20	31.80	34
Ribes 10	62.12	1256866	82.29	17.71	54
Ribes 11	33.32	1194023	61.12	38.88	99
Ribes 12	52.52	3147426	87.08	12.92	70
Ribes 13	46.18	3258674	79.56	20.44	92
Ribes 14	56.13	644626	83.33	16.67	21

Table 3 gives five properties of each of the 34 plant point clouds in the dataset: 1) Plant height, 2) Total number of points, 3) Percentage of "leaf" points, 4) Percentage of "stem" points, and 5) Number of individual leaflets. Plant height is in the range of 25 to 105cm. The number of points exceed 1 million for most plants. Number of individual leaflets varies between 25 to 105, indicating the variation of complexity in plant structure.

2.4 Methods for semantic segmentation

Harandi et al. [22] provided a comprehensive review of typical steps involved in the processing and analysis of 3D representations of plants, including point clouds. Models in PLANesT-3D can be used to evaluate a diverse set of tools developed for plant analysis and phenotyping. In this study, we focus on the application of segmentation of 3D point clouds of plants into their semantic units.

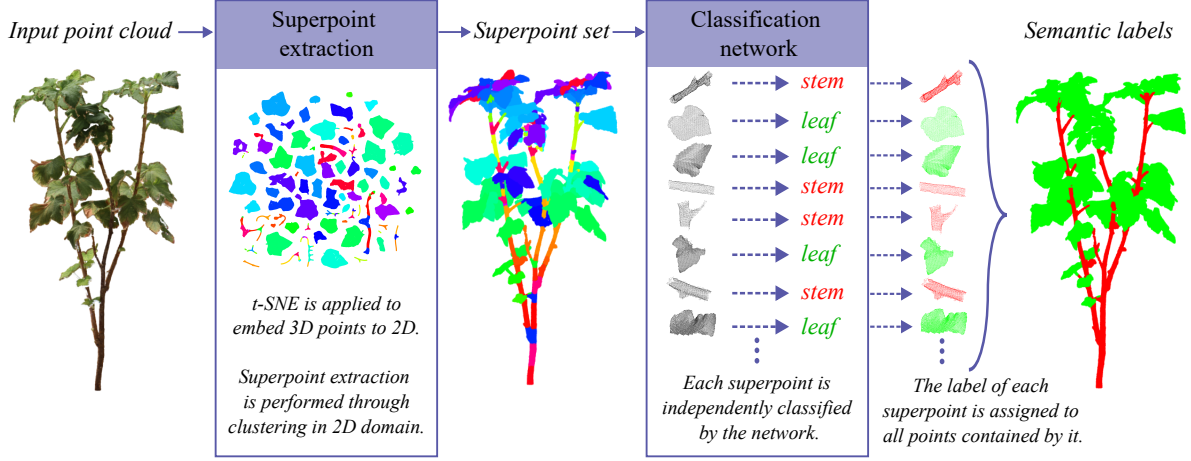


Figure 4: Flowchart of SP-LSCnet. The input point cloud is first passed through the superpoint extraction procedure. This procedure involves embedding of the 3D points into 2D and partitioning the 2D points into superpoints. Once the superpoint assignments are mapped to 3D domain, each superpoint is passed independently through a leaf-stem classification network. The 3D points in a superpoint are all labeled with the global class of the superpoint predicted by the network.

The objective of semantic segmentation is to assign each point p in the point set \mathcal{P} one of the semantic labels. The semantic categories in the PLANesT-3D dataset correspond to "leaf" and "stem", where "leaf" points are on leaf blades, and "stem" points belong to the main stem, branches, and petioles.

We developed a novel semantic segmentation method that is a combination of a superpoint extraction scheme [38] and an adaptive 3D object classification network [45]. We abbreviate this method as SP-LSCnet, where SP stands for superpoint, while LSCnet is a leaf-stem classification network. In order to provide reference performance results for further research, we also tested PointNet++ [46] and RoseSegNet [40] on the new PLANesT-3D dataset.

2.4.1 SP-LSCnet

SP-LSCnet consists of two stages: Superpoint extraction and leaf-stem classification. In superpoint extraction stage, the point cloud is over-segmented into superpoints through an unsupervised process that operates on 2D points embedded by t-SNE. Then, each superpoint generated in the first stage is classified through a deep neural network equipped with attention-based modules that adaptively determine receptive fields for feature extraction. The flowchart of the method is depicted in Fig. 4, and the details of the two stages are given below:

Superpoint extraction: For accomplishing this task, the superpoint extraction scheme proposed in [38] is selected. The plant point cloud is first downsampled with voxel grid average filtering. t-SNE, as introduced in [47], is used to embed the downsampled 3D point cloud into 2D space. Superpoint extraction is then performed exclusively in 2D domain. t-SNE inherently provides clusters that are formed based on the implicit manifolds to which the 3D points belong.

The first step of the superpoint extraction scheme corresponds to the identification of these clusters by Euclidean clustering in 2D. Line-like structures are detected through examining the local geometry of the points. An iterative procedure that involves spectral clustering and solidity computation is employed to segment non-convex clusters into convex regions. Once all 2D points are assigned to their corresponding superpoints, the assignments are carried to their 3D counterparts, and propagated to the high-resolution point cloud through nearest neighbor interpolation.

In this work, for the PLANesT-3D dataset, the grid size for voxel grid average filtering is selected as 0.12cm, the *Perplexity* for t-sNE embedding is set to 30. The distance threshold used in Euclidean clustering in 2D space is chosen as 1. The other parameters were kept in their default settings as given in [38].

Leaf-stem classification network: Each superpoint generated by the previous step is considered to be a separate point cloud. A point-based deep neural network, introduced by [45], is utilized to classify the superpoints into leaf and stem classes (Fig. 4). The network is formed through integrating two modules to the PointNet++ architecture for object classification (Fig. 5). The modules are based on attention mechanisms to analyze point interactions within and between point neighborhoods, and are named as Center Shift Module (CSM) and Radius Update Module (RUM) [45]. Their

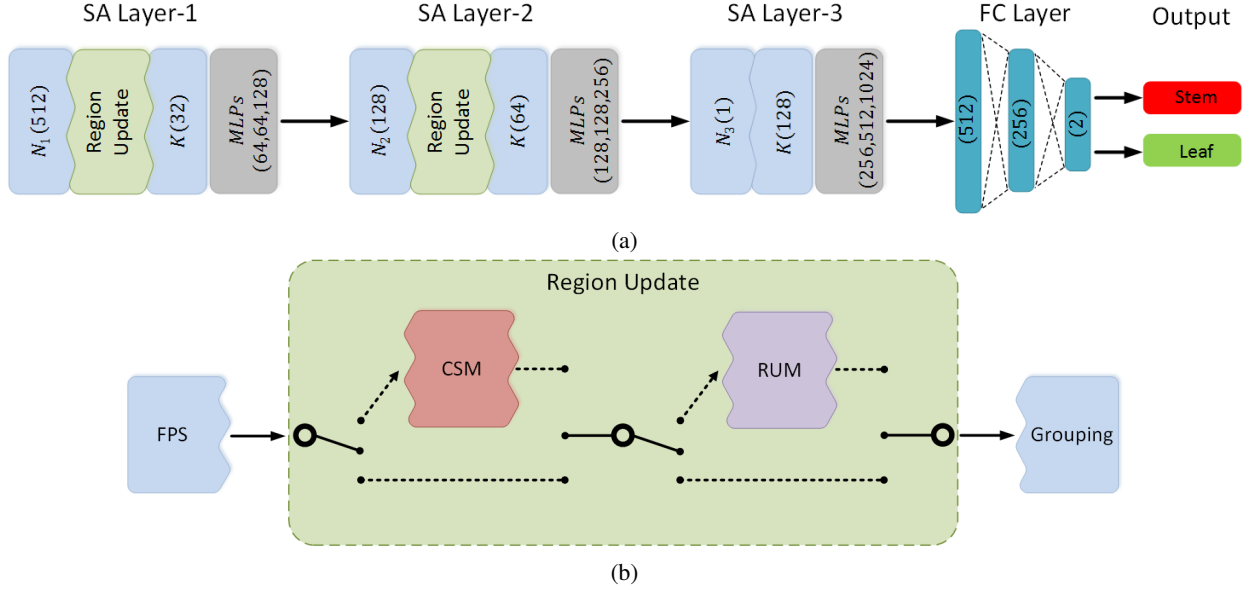


Figure 5: The integration of CSM and RUM to PointNet++ framework [45]: a) The classification network. r^L for $L = 1$ (first layer) is set to be 0.2. r^L for $L = 2$ (second layer) is 0.4. b) Adaptive local region inference with CSM and RUM.

task is to update adaptively the centers and radii of the spherical regions on which PointNet++ encodes local features. This operation is referred to as adaptive local region inference [45].

The classification network architecture of PointNet++ [46], shown in Fig. 5a, includes three set abstraction (SA) layers. The input point cloud with $N = 1024$ points is reduced to $N_1 = 512$, and $N_2 = 128$ representative points during SA layer-1 and SA layer-2, respectively. At each SA layer L , the representative points c_j^L are selected using farthest point sampling (FPS) algorithm. N_L spherical local regions with radius r^L is defined around the center points c_j^L . Within each region, K points are randomly selected and the features of K points are mapped to higher dimensions with MLPs. The abstracted features of each local region are calculated by taking the maximum among the feature channels of K grouped points.

The global descriptors representing the input point cloud are extracted at the last layer, where a single region enclosing the entire object is encoded. The global descriptors are passed through fully connected layers to compute the category scores. In this study, the classification network calculates two category scores for each input point cloud: One for the "leaf" category, and one for the "stem" category.

The adaptive local inference modules, CSM and RUM can be integrated to either or both of the first two layers as shown in Fig. 5b. If CSM is "ON" at a particular layer, for each representative point c_j^L , CSM calculates the shift amount Δc_j^L , through attention-based subnetworks. The representative point is updated as:

$$\hat{c}_j^L = c_j^L + \Delta c_j^L. \quad (4)$$

If RUM is "ON", it computes the amount of radius update Δr_j^L for each region j . The new radius then becomes:

$$\hat{r}_j^L = r^L + \Delta r_j^L. \quad (5)$$

The grouping and feature encoding by MLPs of K points are then performed using these new region definitions. These modules allow the receptive fields to be adaptively shifted and resized through examining local and global point interactions through attention. The network thus adjusts the receptive fields and encodes the 3D points in them in accordance with the main task of the network.

Various alternatives of CSM and RUM were suggested by [45]. As a result of experimental trials, the CSM-II (sub) and RUM-II (cum) versions were selected for the PLANesT-3D dataset. Please, refer to [45] for detailed descriptions of the modules CSM-II (sub) and RUM-II (cum).

2.4.2 PointNet++

We adopted the PointNet++ architecture [46] for semantic segmentation of large point clouds. The data preparation for PointNet++ involves two operations: Subsampling and partitioning the big point set into subsets enclosed by blocks.

The subsampling is performed using voxel-grid filtering, where the edge length of the voxel cube is set as $1mm$. Each voxel is represented with a single point which is the average of the original points occupying the voxel. The sampled point is assigned the label of the closest point in the original cloud. This subsampling operation produces a point cloud with reduced size and homogeneous point density.

3D point-based deep neural networks requires input clouds with a fixed number of points. One way is to subsample the full plant point cloud to have the required number of points. However, such strategy will result in significant loss of geometric information, especially for small structures. Instead, we selected to partition the plant point cloud into subsets of points, each of which is then processed by the network individually. We followed a similar procedure of partitioning the point clouds into blocks as in [34, 40].

The horizontal region, i.e. the extent of the XY plane, encompassing the point cloud is partitioned into squares of edge length of $10cm$. All points with x and y coordinates falling into a square region is considered belonging to the point subset within a block. The points in the block are subsampled to obtain a cloud of fixed number of points, as $N = 8192$. The partitioning operation is conducted twice for each plant point cloud with offset values 0 and $5cm$.

We used the default PointNet++ architecture for semantic segmentation as given in [46]. PointNet++ segmentation network is composed of five grouping/abstraction layers. The radius parameter, which defines the size of local regions for grouping and abstraction, is set for each of the first four layers as $0.5cm$, $1cm$, $2cm$, and $4cm$, respectively. During training, batch size was selected as 16 . The learning rate was updated as 0.005 . Other hyperparameters of the PointNet++ were kept at default values.

2.4.3 RoseSegNet

RoseSegNet was developed for the specific application of semantic segmentation of rosebush models. It involves attention-based modules that encode point interactions within and between local regions. The details of the RoseSegNet architecture can be found in [40].

As with the case of PointNet++, we partition the plant point cloud into blocks and the point subset in each block is separately processed by RoseSegNet. The block partitioning process is the same as with PointNet++.

All the hyperparameters of the RoseSegNet are kept at their default values as given in [40], where the parameter search was performed on the ROSE-x dataset [26].

3 Results

In this section, we provide semantic segmentation results on the PLANesT-3D dataset obtained by the three methods described in Section 2.4. We trained a separate network for each of the three plant species. The hyperparameters of the networks were kept fixed for all the species. 70% of the point clouds were selected for training the networks. The rest is reserved for test. The split for training and test sets for the three species are given in Table 4. The IDs of the plants in the test sets are also provided.

Table 4: The split for training and test sets

Species	Pepper	Rose	Ribes
# plants for training	7	7	10
# plants for test	3	3	4
Plant IDs reserved for test	01, 03, 07	01, 03, 09	03, 10, 11, 14

Table 5: Number of point subsets used for training and test.

Species	Pepper	Rose	Ribes
# training blocks for PointNet++ & RoseSegNet	294	317	665
# test blocks for PointNet++ & RoseSegNet	123	106	205
# training superpoints for SP-LSCnet	1188	933	2761
# test superpoints for SP-LSCnet	646	438	998

Before being processed by the networks, the point clouds were filtered such that points with confidence values less than 6 were discarded. For PointNet++ and RoseSegNet, the point cloud of a plant is partitioned into blocks and each block is separately processes as described in Section 2.4.2. For SP-LSCnet, the point clouds are partitioned into superpoints, and the superpoints are treated as separate objects for the object classification network. Table 5 gives the number of point subsets used for training and test for each plant species.

Table 6: Semantic segmentation results of the three methods on the PLANesT-3D dataset.

	PEPPER		
	PointNet++	RoseSegNet	SP-LSCnet
Precision - Stem	96.5	97.0	97.6
Recall - Stem	94.6	96.1	94.5
IoU - Stem	91.5	93.2	92.4
Precision - Leaf	98.3	98.7	98.3
Recall - Leaf	98.9	99.0	99.3
IoU - Leaf	97.2	97.8	97.6
Acc	97.9	98.3	98.1
MIoU	94.3	95.5	95.0
	ROSE		
	PointNet++	RoseSegNet	SP-LSCnet
Precision - Stem	92.4	94.8	96.4
Recall - Stem	89.7	91.4	85.6
IoU - Stem	83.5	87.1	83.0
Precision - Leaf	97.6	98.0	97.2
Recall - Leaf	98.3	98.8	99.4
IoU - Leaf	96.0	96.9	96.6
Acc	96.7	97.4	97.1
MIoU	89.8	92.0	89.8
	RIBES		
	PointNet++	RoseSegNet	SP-LSCnet
Precision - Stem	95.8	95.9	96.7
Recall - Stem	94.0	95.5	94.0
IoU - Stem	90.3	91.7	91.1
Precision - Leaf	98.9	99.2	98.5
Recall - Leaf	99.2	99.2	99.2
IoU - Leaf	98.1	98.4	97.8
Acc	98.4	98.6	98.3
MIoU	94.2	95.1	94.5

We report the semantic segmentation results of the three methods in Table 6. Precision, Recall, and Intersection over Union (IoU) measures specific to "stem" and "leaf" classes are given in the table, as well as overall accuracy (Acc) and mean IoU (MIoU). In terms of overall accuracy and mean IoU, RoseSegNet yielded the best performance for all three species. For MIoU, RoseSegNet surpassed the performance of PointNet++ by close to 1%. SP-LSCnet is in between, performing slightly better than PointNet++ for the Pepper and Ribes sets, while yielding similar performance to that of PointNet++ for the Rose set.

The results on rose plant models are lower compared to those obtained on pepper and ribes plants. The recall of the "stem" class is more challenging for the rose plant models, since the petioles in between the leaflets are hard to discern. The misclassifications of petiole points of roses as belonging to leaf blades are observable in Fig. 6 and Fig. 7 where segmentation results are visually depicted for sample plants.

Other examples to erroneous cases are given in Fig. 7. The errors produced by PointNet++ and RoseSegNet appear as isolated points scattered in particular regions. Although context information heavily influences the features of single points in PointNet++ and RoseSegNet, the classification is performed individually for each point. Misclassifications occur particularly at cluttered regions where leaves and stems are close to each other.

The treatment of each superpoint as a single entity by SP-LSCnet produces smooth results; however, it suffers from two disadvantages: First, the superpoints might not be always homogeneous; some leakage from other classes is inevitable due to the unsupervised nature of superpoint extraction. Second, the correct classification of the superpoints becomes particularly critical. As can be seen in Fig. 7, portions of the stem were classified as leaf points if the single superpoint to which they belong has the geometrical characteristics of leaves as modeled by the network. Likewise, small leaves, where the point resolution is not sufficient for proper sampling of the leaf surface, are classified as stem. Low point

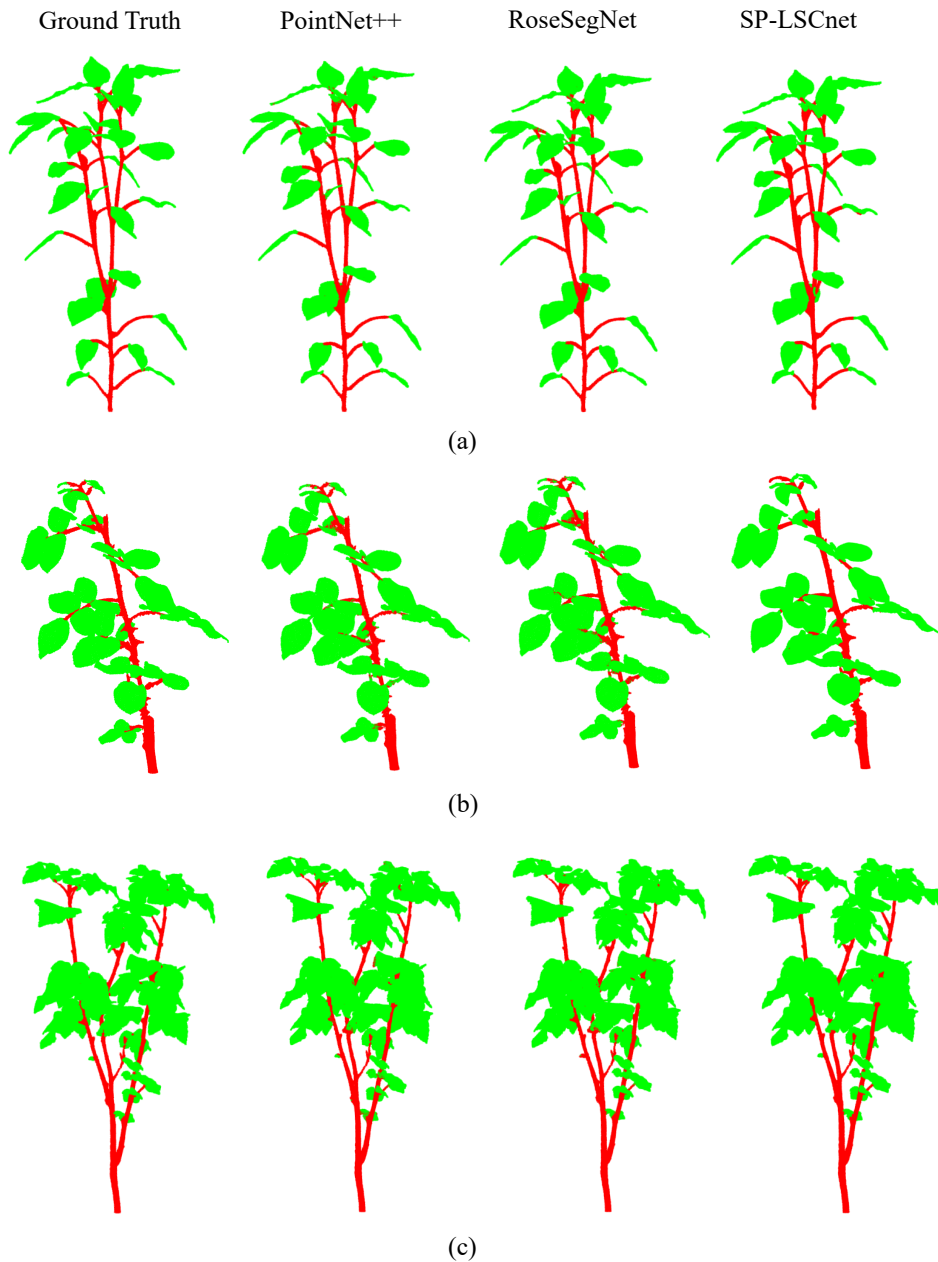


Figure 6: Semantic segmentation results by PointNet++, RoseSegNet, SP-LSCnet, on sample pepper (a), rose (b), and, ribes (c) plants. First column corresponds to the ground truth.

resolution due to occlusion (see bottom-left example in Fig. 7) can also cause isolated regions separated into superpoints which are not large enough to possess distinguishing shapes.

All three methods can benefit from post-processing such as label smoothing for PointNet++ and RoseSegNet, and graph-based re-evaluation of superpoint predictions for SP-LSCnet. However, the limitations of these methods in dealing with scarce annotated data, noisy point clouds, complex architecture of plants, and variable point density call for further developments in plant segmentation methods.

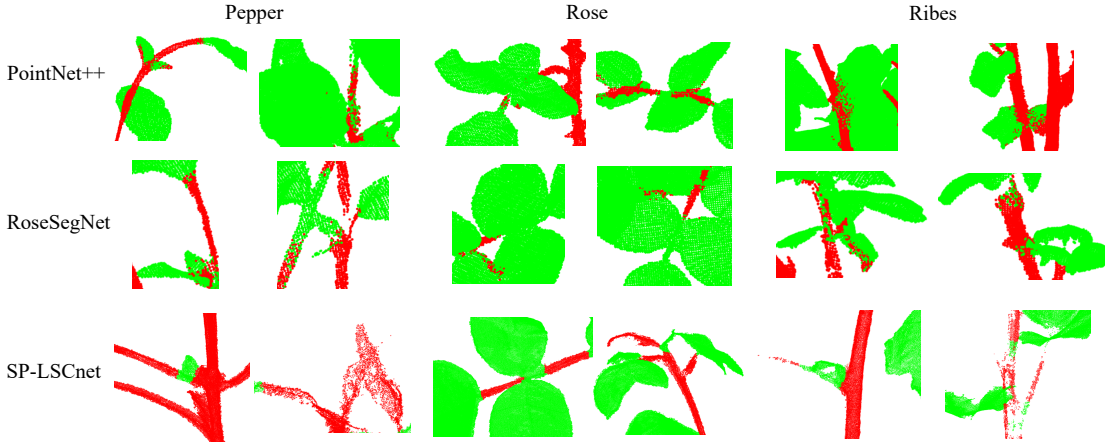


Figure 7: Examples to errors

4 Discussion

The PLANesT-3D dataset is composed of 3D point clouds of plants reconstructed through structure from motion and multi-view stereo. Capturing 3D geometry through SfM has many advantages such as low cost setup requirements, high resolution, and provision of color information [22]. It can be used both in controlled environments and in the field without extensive training for acquisition and elaborate protocols. A public dataset obtained through this modality as opposed to laser scanning is expected to be instrumental in assessing the robustness of 3D plant processing and phenotyping tools.

As can be observed in Table 3, the size of each model in terms of number of points is high, ranging from 600K to 5.5M points. One question is whether such high resolution is necessary for certain tasks related to plant analysis and management. The number of points can be reduced systematically through downsampling to measure the effect of resolution on the performance of particular 3D shape processing tools [48].

We also used quite large numbers of images of the plants for reconstruction (2). This amount of image capture might not be feasible in cases where manual data acquisition is performed. However, advances in robotics enable fast acquisition with autonomous crop surveying robots equipped with robotic arms and multiple cameras [8, 49, 50], as well as techniques for automatic positioning of the robot arms for optimal data acquisition [51]. Nevertheless, limiting the number of images for reconstruction without a performance degradation in particular tasks would substantially reduce the computational demand.

Another important aspect of the new dataset is the availability of color information. Although not demonstrated in this work, use of color information together with 3D geometry can boost the performance of a segmentation procedure [52]. The PLANesT-3D dataset will be a valuable resource for measuring the contribution of color information for automated plant analysis and phenotyping tasks.

Semantic parts annotated in the PLANesT-3D dataset are limited to "leaf" and "stem" classes; however, a more fine-grained annotation is possible, for example, in terms of "leaf blades", "petioles", "main stem", "nodes", and "internodes" [53]. Leaflets, together with petioles, can be grouped into their corresponding individual leaves. The architecture of each plant can be modeled with a graph representation. We envision undertaking this level of annotation as a future work.

Another possible future work is a study on the transferability of the neural network models learned from a plant species into another species. In the current work, we trained a separate network for each of the three plant species. The extent of generalization ability of network models among plant species is of special interest; since manual annotation of plants for training is highly labor-intensive. PLANesT-3D, with a collection of three different species, allows application and evaluation of algorithms such as small sample learning and, transfer learning.

5 Conclusions

We introduced the PLANesT-3D dataset, which is composed of annotated color point clouds of 34 plants belonging to three different species. We described the acquisition, reconstruction, and labeling processes involved in dataset construction. As a use case of the dataset, we reported semantic segmentation results yielded by PointNet++, RoseSegNet, and a novel method abbreviated as SP-LSCnet. RoseSegNet achieved highest segmentation performance, reaching 95.5 %, 92.0 %, and 95.1 % MIOU, for pepper, rose, and ribes plants, respectively. SP-LSCnet also produced comparable results as 95.0 %, 89.8 %, and 94.5 % MIOU on the three plant species. We illustrated sample cases where the three methods failed to produce correct results. The PLANesT-3D dataset will be instrumental for developing new methods that effectively address these challenges.

Acknowledgements:

The authors acknowledge the support of The Scientific and Technological Research Council of Turkey (TUBITAK), Project No: 121E088.

Declaration of Competing Interest

The authors declare that they have no known competing financial interests or personal relationships that could have appeared to influence the work reported in this paper.

References

- [1] L. Riisgaard, N. Hammer, Prospects for labour in global value chains: Labour standards in the cut flower and banana industries, *British Journal of Industrial Relations* 49 (2011) 168–190. doi:<https://doi.org/10.1111/j.1467-8543.2009.00744.x>.
- [2] G. Van den Broeck, M. Maertens, Horticultural exports and food security in developing countries, *Global Food Security* 10 (2016) 11–20. doi:<https://doi.org/10.1016/j.gfs.2016.07.007>.
- [3] S. Tyagi, S. Sahay, M. Imran, K. Rashmi, S. S. Mahesh, Pre-harvest factors influencing the postharvest quality of fruits: A review, *Curr. J. Appl. Sci. Technol* 23 (2017) 12.
- [4] C. W. Bac, E. J. van Henten, J. Hemming, Y. Edan, Harvesting robots for high-value crops: State-of-the-art review and challenges ahead, *Journal of Field Robotics* 31 (2014) 888–911. doi:<https://doi.org/10.1002/rob.21525>.
- [5] R. Bogue, Robots poised to revolutionise agriculture, *Industrial Robot: An International Journal* 43 (2016) 450–456. doi:<https://doi.org/10.1108/IR-05-2016-0142>.
- [6] M. Zhang, Y. Han, D. Li, S. Xu, Y. Huang, Smart horticulture as an emerging interdisciplinary field combining novel solutions: Past development, current challenges, and future perspectives, *Horticultural Plant Journal* (2023). doi:<https://doi.org/10.1016/j.hpj.2023.03.015>.
- [7] E. J. van Henten, A. Tabb, J. Billingsley, M. Popovic, M. Deng, J. Reid, Agricultural robotics and automation [TC Spotlight], *IEEE Robotics and Automation Magazine* 29 (2022) 145–147. doi:<https://doi.org/10.1109/MRA.2022.3213136>.
- [8] A. Atefi, Y. Ge, S. Pitla, J. Schnable, Robotic technologies for high-throughput plant phenotyping: Contemporary reviews and future perspectives, *Frontiers in Plant Science* 12 (2021). doi:<https://doi.org/10.3389/fpls.2021.611940>.
- [9] R. Pieruschka, U. Schurr, Plant phenotyping: Past, present, and future, *Plant Phenomics* 2019 (2019) 7507131. doi:<https://doi.org/10.34133/2019/7507131>.
- [10] K. M. F. James, D. J. Sargent, A. Whitehouse, G. Cielniak, High-throughput phenotyping for breeding targets—Current status and future directions of strawberry trait automation, *Plants, People, Planet* 4 (2022). doi:<https://doi.org/10.1002/ppp3.10275>.
- [11] M. Minervini, H. Schar, S. A. Tsafaris, Image analysis: The new bottleneck in plant phenotyping [applications corner], *IEEE Signal Processing Magazine* 32 (2015) 126–131. doi:<https://doi.org/10.1109/MSP.2015.2405111>.

- [12] S. Kolhar, J. Jagtap, Plant trait estimation and classification studies in plant phenotyping using machine vision – A review, *Information Processing in Agriculture* 10 (2023) 114–135. doi:<https://doi.org/10.1016/j.inpa.2021.02.006>.
- [13] G. R. Y. Coleman, W. T. Salter, More eyes on the prize: open-source data, software and hardware for advancing plant science through collaboration, *AoB PLANTS* 15 (2023) plad010. doi:<https://doi.org/10.1093/aobpla/plad010>.
- [14] V. Zieschank, R. R. Junker, Digital whole-community phenotyping: tracking morphological and physiological responses of plant communities to environmental changes in the field, *Frontiers in Plant Science* 14 (2023). doi:<https://doi.org/10.3389/fpls.2023.1141554>.
- [15] G. Kootstra, X. Wang, P. M. Blok, J. Hemming, E. van Henten, Selective harvesting robotics: Current research, trends, and future directions, *Current Robotics Reports* 2 (2021) 95–104. doi:<https://doi.org/10.1007/s43154-020-00034-1>.
- [16] J. Rong, P. Wang, T. Wang, L. Hu, T. Yuan, Fruit pose recognition and directional orderly grasping strategies for tomato harvesting robots, *Computers and Electronics in Agriculture* 202 (2022) 107430. doi:<https://doi.org/10.1016/j.compag.2022.107430>.
- [17] A. Zahid, M. S. Mahmud, L. He, P. Heinemann, D. Choi, J. Schupp, Technological advancements towards developing a robotic pruner for apple trees: A review, *Computers and Electronics in Agriculture* 189 (2021) 106383. doi:<https://doi.org/10.1016/j.compag.2021.106383>.
- [18] J. Le Louëdec, G. Cielniak, 3D shape sensing and deep learning-based segmentation of strawberries, *Computers and Electronics in Agriculture* 190 (2021) 106374. doi:<https://doi.org/10.1016/j.compag.2021.106374>.
- [19] J. A. Gibbs, M. Pound, A. P. French, D. M. Wells, E. Murchie, T. Pridmore, Approaches to three-dimensional reconstruction of plant shoot topology and geometry, *Functional Plant Biology* 44 (2016) 62–75. doi:<https://doi.org/10.1071/fp16167>.
- [20] S. Paulus, Measuring crops in 3D: Using geometry for plant phenotyping, *Plant methods* 15 (2019) 1–13. doi:<https://doi.org/10.1186/s13007-019-0490-0>.
- [21] F. Okura, 3d modeling and reconstruction of plants and trees: A cross-cutting review across computer graphics, vision, and plant phenotyping, *Breeding Science* 72 (2022) 31–47. doi:<https://doi.org/10.1270/jsbbs.21074>.
- [22] N. Harandi, B. Vandenberghe, J. Vankerschaver, S. Depuydt, A. van Messem, How to make sense of 3D representations for plant phenotyping: a compendium of processing and analysis techniques, *Plant Methods* 19 (2023) 1–46. doi:<https://doi.org/10.1186/s13007-023-01031-z>.
- [23] R. Barth, J. IJsselmuiden, J. Hemming, E. v. Henten, Data synthesis methods for semantic segmentation in agriculture: A *Capsicum annuum* dataset, *Computers and Electronics in Agriculture* 144 (2018) 284–296. doi:<https://doi.org/10.1016/j.compag.2017.12.001>.
- [24] A. Chaudhury, F. Boudon, C. Godin, 3D plant phenotyping: All you need is labelled point cloud data, in: A. Bartoli, A. Fusiello (Eds.), *Computer Vision – ECCV 2020 Workshops*, Springer International Publishing, Cham, 2020, pp. 244–260. doi:https://doi.org/10.1007/978-3-030-65414-6_18.
- [25] D. Schunck, F. Magistri, R. A. Rosu, A. Cornelißen, N. Chebrolu, S. Paulus, J. Léon, S. Behnke, C. Stachniss, H. Kuhlmann, et al., Pheno4D: A spatio-temporal dataset of maize and tomato plant point clouds for phenotyping and advanced plant analysis, *Plos one* 16 (2021) e0256340. doi:<https://doi.org/10.1371/journal.pone.0256340>.
- [26] H. Dutagaci, P. Rasti, G. Galopin, D. Rousseau, ROSE-X: An annotated data set for evaluation of 3D plant organ segmentation methods, *Plant methods* 16 (2020) 1–14. doi:<https://doi.org/10.1186/s13007-020-00573-w>.
- [27] A. Conn, U. V. Pedmale, J. Chory, S. Navlakha, High-resolution laser scanning reveals plant architectures that reflect universal network design principles, *Cell systems* 5 (2017) 53–62. doi:<https://doi.org/10.1016/j.cels.2017.06.017>.
- [28] A. Conn, U. V. Pedmale, J. Chory, C. F. Stevens, S. Navlakha, A statistical description of plant shoot architecture, *Current Biology* 27 (2017) 2078–2088.e3. doi:<https://doi.org/10.1016/j.cub.2017.06.009>.
- [29] A. Conn, A. Chandrasekhar, M. v. Rongen, O. Leyser, J. Chory, S. Navlakha, Network trade-offs and homeostasis in arabidopsis shoot architectures, *PLOS Computational Biology* 15 (2019) 1–19. doi:<https://doi.org/10.1371/journal.pcbi.1007325>.

- [30] Y. Sun, Z. Zhang, K. Sun, S. Li, J. Yu, L. Miao, Z. Zhang, Y. Li, H. Zhao, Z. Hu, D. Xin, Q. Chen, R. Zhu, Soybean-MVS: Annotated three-dimensional model dataset of whole growth period soybeans for 3D plant organ segmentation, *Agriculture* 13 (2023). doi:<https://doi.org/10.3390/agriculture13071321>.
- [31] Y. Lu, S. Young, A survey of public datasets for computer vision tasks in precision agriculture, *Computers and Electronics in Agriculture* 178 (2020) 105760. doi:<https://doi.org/10.1016/j.compag.2020.105760>.
- [32] I. Ziamtsov, S. Navlakha, Machine Learning Approaches to Improve Three Basic Plant Phenotyping Tasks Using Three-Dimensional Point Clouds, *Plant Physiology* 181 (2019) 1425–1440. doi:<https://doi.org/10.1104/pp.19.00524>.
- [33] D. Li, J. Li, S. Xiang, A. Pan, PSegNet: Simultaneous semantic and instance segmentation for point clouds of plants, *Plant Phenomics* 2022 (2022). doi:<https://doi.org/10.34133/2022/9787643>.
- [34] K. Turgut, H. Dutagaci, G. Galopin, D. Rousseau, Segmentation of structural parts of rosebush plants with 3D point-based deep learning methods, *Plant Methods* 18 (2022) 1–23. doi:<https://doi.org/10.1186/s13007-022-00857-3>.
- [35] I. Ziamtsov, S. Navlakha, Plant 3D (P3D): a plant phenotyping toolkit for 3D point clouds, *Bioinformatics* 36 (2020) 3949–3950. doi:<https://doi.org/10.1093/bioinformatics/btaa220>.
- [36] K. Mirande, C. Godin, M. Tisserand, J. Charlaix, F. Besnard, F. Hétyroy-Wheeler, A Graph-Based Approach for Simultaneous Semantic and Instance Segmentation of Plant 3D Point Clouds, *Frontiers in Plant Science* 13 (2022) 1–20. doi:<https://doi.org/10.3389/fpls.2022.1012669>.
- [37] S. Xiang, D. Li, Research on plant growth tracking based on point cloud segmentation and registration, in: 2022 International Conference on Image Processing, Computer Vision and Machine Learning (ICICML), 2022, pp. 469–478. doi:<https://doi.org/10.1109/ICICML57342.2022.10009765>.
- [38] H. Dutagaci, Using t-distributed stochastic neighbor embedding for visualization and segmentation of 3d point clouds of plants, *Turkish Journal of Electrical Engineering and Computer Sciences* 31 (2023) 792–813. doi:<https://doi.org/10.55730/1300-0632.4018>.
- [39] D. Li, G. Shi, J. Li, Y. Chen, S. Zhang, S. Xiang, S. Jin, PlantNet: A dual-function point cloud segmentation network for multiple plant species, *ISPRS Journal of Photogrammetry and Remote Sensing* 184 (2022) 243–263. doi:<https://doi.org/10.1016/j.isprsjprs.2022.01.007>.
- [40] K. Turgut, H. Dutagaci, D. Rousseau, Roseseget: An attention-based deep learning architecture for organ segmentation of plants, *Biosystems Engineering* 221 (2022) 138–153. doi:<https://doi.org/10.1016/j.biosystemseng.2022.06.016>.
- [41] X. Guo, Y. Sun, H. Yang, FF-Net: Feature-fusion-based network for semantic segmentation of 3d plant point cloud, *Plants* 12 (2023). doi:<https://doi.org/10.3390/plants12091867>.
- [42] R. Hartley, A. Zisserman, Multiple view geometry in computer vision, Cambridge university press, 2003.
- [43] P. Torr, A. Zisserman, MLESAC: A new robust estimator with application to estimating image geometry, *Computer Vision and Image Understanding* 78 (2000) 138 – 156. doi:<https://doi.org/10.1006/cviu.1999.0832>.
- [44] D. Girardeau-Montaut, et al., Cloudcompare: 3d point cloud and mesh processing software, *Open Source Project* 197 (2015). URL: <http://www.cloudcompare.org/>.
- [45] K. Turgut, H. Dutagaci, Local region-learning modules for point cloud classification, 2023. arXiv:2303.17338.
- [46] C. R. Qi, L. Yi, H. Su, L. J. Guibas, PointNet++: Deep hierarchical feature learning on point sets in a metric space, *Advances in neural information processing systems* 30 (2017).
- [47] L. van der Maaten, G. Hinton, Visualizing data using t-SNE, *Journal of machine learning research* 9 (2008).
- [48] A. Chaudhury, P. Hanappe, R. Azais, C. Godin, D. Colliaux, Transferring PointNet++ segmentation from virtual to real plants, in: ICCV 2021 - International Conference on Computer Vision, Montreal, Canada, 2021, pp. 1–3. URL: <https://hal.science/hal-03540304>.
- [49] J. Iqbal, R. Xu, H. Halloran, C. Li, Development of a multi-purpose autonomous differential drive mobile robot for plant phenotyping and soil sensing, *Electronics* 9 (2020). doi:<https://doi.org/10.3390/electronics9091550>.
- [50] C. Smitt, M. Halstead, T. Zaenker, M. Bennowitz, C. McCool, PATHoBot: A robot for glasshouse crop phenotyping and intervention, in: 2021 IEEE International Conference on Robotics and Automation (ICRA), 2021, pp. 2324–2330. doi:<https://doi.org/10.1109/ICRA48506.2021.9562047>.

- [51] C. Wu, R. Zeng, J. Pan, C. C. Wang, Y.-J. Liu, Plant phenotyping by deep-learning-based planner for multi-robots, *IEEE Robotics and Automation Letters* 4 (2019) 3113–3120. doi:<https://doi.org/10.1109/LRA.2019.2924125>.
- [52] F. P. Boogaard, E. J. van Henten, G. Kootstra, Boosting plant-part segmentation of cucumber plants by enriching incomplete 3D point clouds with spectral data, *Biosystems Engineering* 211 (2021) 167–182. doi:<https://doi.org/10.1016/j.biosystemseng.2021.09.004>.
- [53] F. P. Boogaard, E. J. van Henten, G. Kootstra, Improved point-cloud segmentation for plant phenotyping through class-dependent sampling of training data to battle class imbalance, *Frontiers in Plant Science* 13 (2022). doi:<https://doi.org/10.3389/fpls.2022.838190>.